Eur. Phys. J. D **33**, 137–147 (2005)
DOI: 10.1140/epjd/e2005-00030-0

THE EUROPEAN PHYSICAL JOURNAL D

# One-photon and two-photon double-slit interference in spontaneous and stimulated parametric down-conversions

De-Zhong Cao[1], Zhuan Li[1], Yan-Hua Zhai[1], and Kaige Wang[2,1,a]

[1] Department of Physics, Applied Optics Beijing Area Major Laboratory, Beijing Normal University, Beijing 100875, P.R. China
[2] CCAST (World Laboratory), P.O. Box 8730, Beijing 100080, P.R. China

Received 27 July 2004 / Received in final form 17 November 2004
Published online 1st March 2005 – 

**Abstract.** We theoretically discuss two-photon double-slit interference for spontaneous and stimulated parametric down-conversions and compare it with one-photon case. We show that two-photon sub-wavelength interference can exist in a general interaction of spontaneous parametric down-conversion (SPDC) for both type I and type II crystals. In low gain SPDC, interference effect can be attributed to the previous study based on two-photon entangled state. But the important fact is that the sub-wavelength interference will not be washed out even if in very high gain SPDC, revealing the macroscopic nature. We propose an alternative scheme to observe sub-wavelength interference with a joint-intensity measurement, which occurs for a type I crystal in the high gain case. The theoretical analysis shows that the effect originates from classical thermal correlation. However, we also formulate the one-photon and two-photon double-slit interference in the stimulated process, and show amplified interference patterns.

**PACS.** 42.50.Dv Nonclassical states of the electromagnetic field, including entangled photon states; quantum state engineering and measurements – 42.65.Lm Parametric down conversion and production of entangled photons – 42.25.Hz Interference – 42.82.Cr Fabrication techniques; lithography, pattern transfer

## 1 Introduction

Young's double-slit interference experiment is one of the powerful ways to exhibit the nature of optical field, including both classical and nonclassical coherence effects. In recent years, an interesting subject is devoted to the study of two-photon double-slit interference in the process of spontaneous parametric down-conversion (SPDC) [1–15]. Since in this process a pair of converted beams generated by a pump beam are entangled, the two-photon double-slit interference may show some peculiar phenomena such as sub-wavelength interference (or quantum lithography) and ghost interference. For the former, both signal and idler beams are set together to pass through a double-slit [5,6,8–11,13,14] and for the latter, the double-slit is placed on a path of only one beam [1–4,7,12,15]. The original idea of the sub-wavelength interference comes from the reduction of de Broglie wavelength for combining two massive particles. It was extended to optical interference for a biphoton or multi-photon state in a beam splitter and a Mach-Zehnder interferometer [16–20]. Due to the fact that this effect can surpass the Rayleigh diffraction limit, it may have prospective application in photo-lithography technology.

In most of theoretical analyses, the sub-wavelength interference is explained by a two-photon entangled state which can be acquired in low gain SPDC. Nevertheless, the low intensity is the obstacle in practical application. Therefore, the exploration of these effects in macroscopic regime makes sense [15,18,19]. References [18,19] showed that in high gain SPDC the sub-wavelength interference can occur in a Mach-Zehnder interferometer. This effect implies that two-photon entanglement can persist macroscopically. However, recent studies [21,22] proposed that it is possible to perform coherent imaging by using the classical correlation of two beams obtained by splitting incoherent thermal radiation. Gatti et al. [21,22] indicated there is a formal analogy between two classically correlated beams and two entangled beams produced by parametric down-conversion. Because of this analogy, the classical beams can mimic qualitatively all the imaging properties of the entangled beams. In addition, they also pointed out that the sub-wavelength double-slit interference could in principle be observed in the scheme that uses the classically correlated thermal beams, provided that the pixels in the detection planes of the two beams are scanned symmetrically [21]. In parallel, reference [23] theoretically demonstrated that a thermal light source which is random in the transverse direction can produce a sub-wavelength double-slit interference in a joint intensity measurement.

[a] e-mail: wangkg@bnu.edu.cn

In this paper, we study one-photon and two-photon double-slit interference in both spontaneous and stimulated parametric down-conversions. We focus on the case in which a double-slit is placed on the paths of both signal and idler beams. We find that sub-wavelength lithography can occur in very high gain SPDC with substantial visibility. The discussion covers both type I and type II crystals which exhibit different behavior in two-photon interference. For a type I crystal, we demonstrate that the sub-wavelength double-slit interference can occur in two kinds of observation, with both a two-photon intensity measurement and a joint-intensity measurement in which two one-photon detectors are placed at symmetric positions with respect to the double-slit. The former originates from quantum two-photon entanglement, and the latter from classical thermal spatial correlation which exists only in high gain SPDC. We also formulate one-photon and two-photon double-slit interference for stimulated parametric down-conversion. The paper is organized as follows: in Section 2 we briefly review double-slit interference for a coherent state and a two-photon state. In Section 3 we cite several formulas as a review of the optical parametric down-conversion process. We analyze two-photon double-slit interference in Sections 4 and 5 for the spontaneous and stimulated processes, respectively. The final Section 6 is the conclusion and discussion.

## 2 Double-slit interference for a coherent state and a two-photon state

We consider the scheme of Young's double-slit experiment as shown in Figure 1. The double-slit function is defined by

$$T(x) = \begin{cases} 1 & (d-b)/2 \le |x| \le (d+b)/2, \\ 0 & \text{others}, \end{cases} \tag{1}$$

where $d$ is the distance between the centers of two slits and $b$ is the width of each slit. In Figure 1, both the double-slit and the detection screen are placed at the two focal planes of a lens. By ignoring the thickness of the double-slit and taking into account $T^2(x) = T(x)$, the outgoing transverse envelope operator $e'(x,t)$ of the double-slit is written as

$$e'(x,t) = T(x)e(x,t) + [1 - T(x)]e_{vac}(x,t), \tag{2}$$

where $e(x,t)$ is the field injected into the double-slit and the vacuum field operator $e_{vac}(x,t)$ is introduced for the sake of $e'(x,t)$ satisfying the bosonic commutation relation. Since the vacuum field has no contribution to the normal-order correlation, it can be neglected in the calculations below.

In the paraxial approximation, the field $r(x,t)$ in the detection plane $P_2$ is expressed by a Fourier transform of the lens

$$r(x,t) = \sqrt{\frac{k}{2\pi f}} \int e'(x',t) \exp\left[-i\frac{k}{f}x'x\right] dx'. \tag{3}$$

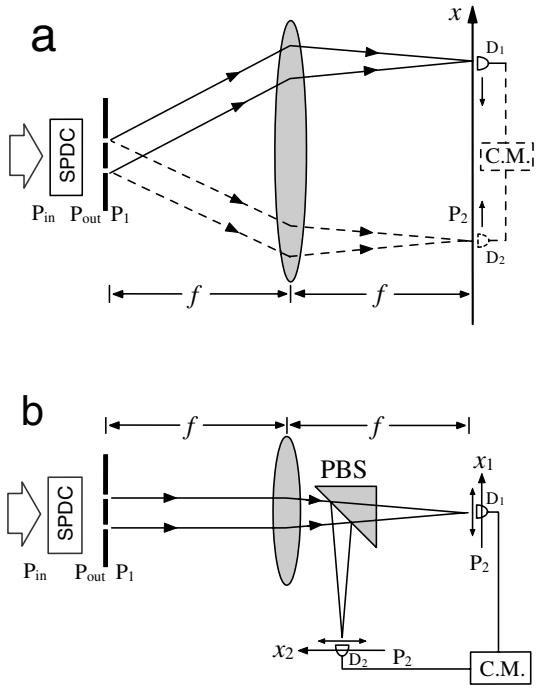


**Fig. 1.** Schemes of Young's double-slit interference with a convex lens: (a) a one-photon (two-photon) detector measures one-photon (two-photon) intensity distribution; two one-photon detectors measure joint-intensity distribution at a pair of symmetric positions. (b) for a type II crystal, two-photon intensity distribution is measured by two one-photon detectors through a polarizing beam splitter (PBS).

By substituting equation (2) into equation (3), we obtain

$$r(x,t) = \frac{1}{2\pi}\sqrt{\frac{k}{f}} \int \widetilde{T}\left(\frac{kx}{f} - q\right) \widetilde{e}(q,\Omega) \exp[-i\Omega t] dq d\Omega, \tag{4}$$

where

$$\widetilde{T}(q) = \frac{1}{\sqrt{2\pi}} \int T(x) e^{-iqx} dx = \frac{2b}{\sqrt{2\pi}} \operatorname{sinc}(qb/2) \cos(qd/2) \tag{5}$$

is the Fourier transform of the double-slit function $T(x)$, and $\widetilde{e}(q,\Omega)$ is the Fourier transform of $e(x,t)$ for both the spatial and temporal variables.

To begin with, we consider the field $e(x,t)$ to be a stationary and monochromatic plane wave in a coherent state

$$\langle e(x,t) \rangle = A, \tag{6}$$

where $A$ is a constant. When the field is normally incident onto the double-slit, it has

$$\langle \widetilde{e}(q,\Omega) \rangle = 2\pi A \delta(q) \delta(\Omega). \tag{7}$$

In the detection plane, the first-order correlation is calculated as

$$\begin{aligned} G^{(1)}(x_1,x_2,t) &\equiv \langle r^\dagger(x_1,t) r(x_2,t) \rangle \\ &= \frac{kA^2}{f} \widetilde{T}^* \left(\frac{kx_1}{f}\right) \widetilde{T}\left(\frac{kx_2}{f}\right). \end{aligned} \tag{8}$$

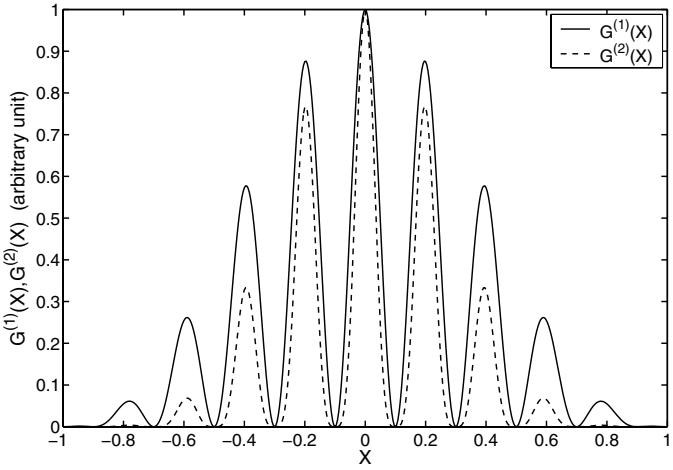


**Fig. 2.** One-photon (solid line) and two-photon (dashed line) double-slit interference patterns for a coherent beam.

Hence, the intensity distribution in the detection plane is written as

$$G^{(1)}(x,x,t) \equiv \left\langle r^{\dagger}(x,t)r(x,t)\right\rangle = \frac{kA^2}{f}\widetilde{T}^2\left(\frac{kx}{f}\right) = I_0 \mathrm{sinc}^2\left(\frac{\pi bx}{\lambda f}\right)\cos^2\left(\frac{\pi dx}{\lambda f}\right), \quad (9)$$

where $I_0 = 2kb^2A^2/(\pi f)$ and $\lambda = 2\pi/k$. Note that $\widetilde{T}(x)$ is a real function. Equation (9) represents an interference fringe with the interval $\lambda f/d$ in the range $\lambda f/b$, as shown in Figure 2.

Similarly, the second-order correlation function can be obtained as

$$G^{(2)}(x_1,x_2,t) = \left\langle r^{\dagger}(x_1,t)r^{\dagger}(x_2,t)r(x_2,t)r(x_1,t)\right\rangle = \frac{k^2A^4}{f^2}\widetilde{T}^2\left(\frac{kx_1}{f}\right)\widetilde{T}^2\left(\frac{kx_2}{f}\right). \quad (10)$$

According to the theory of field coherence, the separability of spatial variables in correlation functions verifies perfect coherence of the field. Since the field operators at different positions are commutable, the second-order correlation of the field at $x_1 \neq x_2$ is in fact the spatial intensity correlation and it can be observed by joint-intensity measurement as shown in Figure 1a. The spatial patterns related to $G^{(1)}(x,x,t)$ and $G^{(2)}(x_1,x_2,t)$ are called the one-photon and two-photon interference, respectively. According to equation (10), in the joint-intensity measurement, if we scan one detector while fix the other, the same interference fringe as the one-photon interference can be observed. We now introduce two kinds of observation for the two-photon double-slit interference. One is the spatial intensity-correlation measurement by scanning two detectors synchronously at a pair of symmetric positions, $x_1 = -x_2 = x$. The other one is the two-photon intensity measurement by using a two-photon detector which generates a photo-electron by absorbing two photons. Applying these two kinds of observation to equation (10), we obtain

$$G^{(2)}(x,x,t) = G^{(2)}(x,-x,t) = I_0^2 \mathrm{sinc}^4\left(\frac{\pi bx}{\lambda f}\right)\cos^4\left(\frac{\pi dx}{\lambda f}\right). \quad (11)$$

In Figure 2, we plot $G^{(2)}(x,x,t)$ ($G^{(2)}(x,-x,t)$) in comparison with $G^{(1)}(x,t)$ for the coherent beam: the two interference patterns are alike.

The above discussion on the coherent state is analogous to a classical field. Then, we consider a two-photon state as input, which is a quantum state without classical analogy. A general two-photon state can be written as

$$|\psi\rangle = \int dq_s dq_i C(q_s,q_i)a_s^{\dagger}(q_s)a_i^{\dagger}(q_i)|0\rangle, \quad (12)$$

where $a_s^{\dagger}$ and $a_i^{\dagger}$ are respectively the creation operators for $s$ and $i$ photons which are assumed to be distinguishable. $q_s$ and $q_i$ are the transverse wavevectors. When the input field is stationary, equation (4) can be simplified as

$$r(x) = \sqrt{\frac{k}{2\pi f}}\int \widetilde{T}\left(\frac{kx}{f}-q\right)\widetilde{e}(q)dq. \quad (13)$$

By using equation (13), the first-order correlation functions for $s$-photon and $i$-photon in the detection plane are obtained as

$$G_s^{(1)}(x_1,x_2) = \frac{k}{2\pi f}\int dq dq_1 dq_2 C^*(q_1,q)C(q_2,q) \times \widetilde{T}^*\left(\frac{kx_1}{f}-q_1\right)\widetilde{T}\left(\frac{kx_2}{f}-q_2\right), \quad (14a)$$

$$G_i^{(1)}(x_1,x_2) = \frac{k}{2\pi f}\int dq dq_1 dq_2 C^*(q,q_1)C(q,q_2) \times \widetilde{T}^*\left(\frac{kx_1}{f}-q_1\right)\widetilde{T}\left(\frac{kx_2}{f}-q_2\right), \quad (14b)$$

respectively.

The second-order correlation function for the two modes is defined by

$$G^{(2)}(x_1,x_2,t) = \left\langle r_i^{\dagger}(x_1,t)r_s^{\dagger}(x_2,t)r_s(x_2,t)r_i(x_1,t)\right\rangle, \quad (15)$$

which describes a coincidence probability of $s$-photon at position $x_2$ and $i$-photon at position $x_1$. However, $G^{(2)}(x,x,t)$ describes a two-photon intensity distribution. For the two-photon state (12), we calculate the two-photon wavepacket in the detection plane

$$\langle 0|r_s(x_2)r_i(x_1)|\psi\rangle = \frac{k}{2\pi f}\int dq_s dq_i C(q_s,q_i) \times \widetilde{T}\left(\frac{kx_2}{f}-q_s\right)\widetilde{T}\left(\frac{kx_1}{f}-q_i\right). \quad (16)$$

Hence the second-order correlation can be expressed as

$$G^{(2)}(x_1,x_2) = |\langle 0|r_s(x_2)r_i(x_1)|\psi\rangle|^2. \quad (17)$$

We discuss two extreme cases: two photons are independent and two photons are perfectly entangled in the transverse wavevector. In the non-entangled case, $C(q_s, q_i) = C_s(q_s)C_i(q_i)$, the first- and second-order correlation functions are written as

$$G_m^{(1)}(x_1, x_2) = \frac{k}{2\pi f}\int C_m^*(q)\widetilde{T}^*\left(\frac{kx_1}{f} - q\right)dq \times \int C_m(q)\widetilde{T}\left(\frac{kx_2}{f} - q\right)dq, \quad (m = s, i), \tag{18a}$$

$$G^{(2)}(x_1, x_2) = \left|\frac{k}{2\pi f}\int C_s(q)\widetilde{T}\left(\frac{kx_2}{f} - q\right)dq \times \int C_i(q)\widetilde{T}\left(\frac{kx_1}{f} - q\right)dq\right|^2 = G_i^{(1)}(x_1, x_1)G_s^{(1)}(x_2, x_2). \tag{18b}$$

Equations (18) exhibit the same separability as a coherent state (see Eqs. (8) and (10)), identifying perfect first- and second-order coherence. However, equation (18b) shows the independence of two photons in the second-order correlation, that is, the two-photon interference consists of two individual one-photon interference. This seems to obey the Dirac's statement: "Each photon interferes only with itself. Interference between two different photons never occurs".

In the opposite extreme, we assume perfect wavevector-entanglement in a two-photon state (12), i.e. $C(q_s, q_i) \to \delta(q_s + q_i)$. The first- and second-order correlation functions are written as

$$G_s^{(1)}(x_1, x_2) = G_i^{(1)}(x_1, x_2) = \frac{k}{2\pi f}\int dq\widetilde{T}^*\left(\frac{kx_1}{f} + q\right)\widetilde{T}\left(\frac{kx_2}{f} + q\right) = \frac{k}{f\sqrt{2\pi}}\widetilde{T}\left[\frac{k}{f}(x_2 - x_1)\right], \tag{19a}$$

$$G^{(2)}(x_1, x_2) = \left|\frac{k}{2\pi f}\int dq\widetilde{T}\left(\frac{kx_2}{f} + q\right)\widetilde{T}\left(\frac{kx_1}{f} - q\right)\right|^2 = \frac{k^2}{2\pi f^2}\widetilde{T}^2\left[\frac{k}{f}(x_1 + x_2)\right], \tag{19b}$$

respectively, where we use the integrals

$$\int dq\widetilde{T}^*\left(\frac{kx_1}{f} \pm q\right)\widetilde{T}\left(\frac{kx_2}{f} \pm q\right) = \frac{1}{2\pi}\int dqdx_1'dx_2'T(x_1')T(x_2')e^{i\left(\frac{kx_1}{f}\pm q\right)x_1' - i\left(\frac{kx_2}{f}\pm q\right)x_2'} = \int dx_1'dx_2'T(x_1')T(x_2')\delta(x_1' - x_2')e^{i\frac{kx_1}{f}x_1' - i\frac{kx_2}{f}x_2'} = \int dx_1'T(x_1')T(x_1')e^{i\frac{k}{f}(x_1 - x_2)x_1'} = \sqrt{2\pi}\widetilde{T}\left[\frac{k}{f}(x_2 - x_1)\right] \tag{20}$$

and

$$\int dq\widetilde{T}\left(\frac{kx_1}{f} \pm q\right)\widetilde{T}\left(\frac{kx_2}{f} \mp q\right) = \sqrt{2\pi}\widetilde{T}\left[\frac{k}{f}(x_2 + x_1)\right], \tag{21}$$

and take into account $T^2(x) = T(x)$. Equations (19) show position-correlation and decoherence of the field. In measurement, setting $x_1 = x_2$ in equation (19), we obtain

$$G_s^{(1)}(x, x) = G_i^{(1)}(x, x) = \frac{k}{f\sqrt{2\pi}}\widetilde{T}(0), \tag{22a}$$

$$G^{(2)}(x, x) = \frac{k^2}{2\pi f^2}\widetilde{T}^2\left[\frac{k}{f}(2x)\right]. \tag{22b}$$

Therefore, the one-photon double-slit interference disappears completely and the two-photon double-slit interference shows a sub-wavelength property due to the term

$$\widetilde{T}^2\left(\frac{k}{f}2x\right) \propto \mathrm{sinc}^2\left[\frac{\pi bx}{(\lambda/2)f}\right]\cos^2\left[\frac{\pi dx}{(\lambda/2)f}\right]. \tag{23}$$

The fringe is the same as the ordinary double-slit interference of a coherent beam with half the wavelength. As has been explained, the entangled photon pair should be seen as a biphoton, and the sub-wavelength interference occurs between biphotons. On the other hand, each single photon in biphoton is in a mixed state, causing decoherence. For a general two-photon entangled state, the relation between the first- and second-order correlation functions shows the complementarity of coherence and entanglement [8,10,11]. Finally, we indicate that equations (19) are also valid for the case when $s$ and $i$ photons are indistinguishable.

In Sections 4 and 5, we will see again these basic relations of first- and second-order correlation functions in a general parametric process.

## 3 The basic formula in optical parametric down-conversion

In the optical parametric down-conversion process, in which a plane-wave pump field of frequency $\omega_p$ activates a $\chi^{(2)}$ nonlinear crystal, the basic unitary transformation is described by [15,24–26]

$$\widetilde{e}_m(q, \Omega) = U_m(q, \Omega)\widetilde{a}_m(q, \Omega) + V_m(q, \Omega)\widetilde{a}_n^\dagger(-q, -\Omega) \quad (m \neq n = s, i), \tag{24}$$

where $\widetilde{e}_m(q, \Omega)$ and $\widetilde{a}_m(q, \Omega)$ are the output and input field operators, respectively. $q$ is the transverse wavevector and $\Omega$ is the frequency deviation from the carrier frequency. In the collinear case, the transfer coefficients $U_m(q, \Omega)$ and

$V_m(q,\Omega)$ are given by [26]

$$U_s(q,\Omega) = \Theta_s(q,\Omega)\Big[\cosh\Gamma(q,\Omega) + i\frac{\Delta(q,\Omega)}{2\Gamma(q,\Omega)}\sinh\Gamma(q,\Omega)\Big], \quad (25)$$

$$V_s(q,\Omega) = \Theta_s(q,\Omega)\frac{g}{\Gamma(q,\Omega)}\sinh\Gamma(q,\Omega), \quad (26)$$

$$U_i(q,\Omega) = \Theta_i(q,\Omega)\Big[\cosh\Gamma(-q,-\Omega) + i\frac{\Delta(-q,-\Omega)}{2\Gamma(-q,-\Omega)}\sinh\Gamma(-q,-\Omega)\Big], \quad (27)$$

$$V_i(q,\Omega) = \Theta_i(q,\Omega)\frac{g}{\Gamma(-q,-\Omega)}\sinh\Gamma(-q,-\Omega), \quad (28)$$

where

$$\Theta_m(q,\Omega) = e^{i[k_{mz}(q,\Omega)-k_{nz}(-q,-\Omega)-2k_m+k_p]l_c/2} \quad (m\neq n=s,i), \quad (29)$$

$$\Gamma(q,\Omega) = \sqrt{g^2-\Delta^2(q,\Omega)/4}, \quad (30)$$

$$\Delta(q,\Omega) = [k_{sz}(q,\Omega)+k_{iz}(-q,-\Omega)-k_p]l_c, \quad (31)$$

$$\Delta_0 = (k_s+k_i-k_p)l_c. \quad (32)$$

$g$ is the coupling strength and $l_c$ is the length of crystal. $\Delta_0$ is the collinear phase mismatching of the central frequency components which correspond to the wavenumbers $k_j$ ($j=s,i,p$). For simplicity, we assume that two down-converted beams have the degenerate carrier frequency $\omega_p/2$. Hence, equation (31) can be reduced to [26]

$$\Delta(q,\Omega) \approx \Delta_0 + \Omega^2/\Omega_0^2 + \Omega/\Omega_0' - q^2/q_0^2 - q/q_0', \quad (33)$$

where $\Omega_0$ and $q_0$ are defined as the frequency and spatial-frequency bandwidths, respectively. $\Omega_0'$ and $q_0'$ represent the temporal and spatial walk-off, respectively. The transfer coefficients $U$ and $V$ satisfy the following unitarity conditions [26]

$$|U_m(q,\Omega)|^2 - |V_m(q,\Omega)|^2 = 1 \quad (m=s,i), \quad (34a)$$

$$U_m(q,\Omega)V_n(-q,-\Omega) = U_n(-q,-\Omega)V_m(q,\Omega) \quad (m\neq n=s,i). \quad (34b)$$

Equations (24–33) describe the SPDC process of type II crystals but also can be applicable to type I crystals. For the former, two converted beams are orthogonally polarized, whereas for the latter, they are degenerate in both polarization and central frequency. However, in equation (33), $\Omega_0'\to\infty$ and $q_0'\to\infty$ are set for type I crystals. Therefore, equation (24) can describe type I crystals by omitting the subscripts. As a matter of fact, under the assumption of the carrier frequency degeneracy, equations (25) and (26) are the same as equations (27) and (28), respectively.

Using equation (24), we calculate the first- and second-order correlation functions for the down-converted beams

$$\left\langle \widetilde{e}_m^\dagger(q,\Omega)\widetilde{e}_m(q',\Omega')\right\rangle = |V_m(q,\Omega)|^2\,\delta(q-q')\delta(\Omega-\Omega') \quad (m=s,i) \quad (35a)$$

$$\left\langle \widetilde{e}_i^\dagger(q_1,\Omega_1)\widetilde{e}_s^\dagger(q_2,\Omega_2)\widetilde{e}_s(q_2',\Omega_2')\widetilde{e}_i(q_1',\Omega_1')\right\rangle = V_i^*(q_1,\Omega_1)V_s^*(q_2,\Omega_2)V_s(q_2',\Omega_2')V_i(q_1',\Omega_1') \times[\delta(q_1-q_1')\delta(\Omega_1-\Omega_1')\delta(q_2-q_2')\delta(\Omega_2-\Omega_2') + \delta_{is}\times\delta(q_1-q_2')\delta(\Omega_1-\Omega_2')\delta(q_2-q_1')\delta(\Omega_2-\Omega_1')] + V_i^*(q_1,\Omega_1)U_s^*(q_2,\Omega_2)V_s(q_2',\Omega_2')U_i(q_1',\Omega_1') \times\delta(q_1+q_2)\delta(\Omega_1+\Omega_2)\delta(q_1'+q_2')\delta(\Omega_1'+\Omega_2'), \quad (35b)$$

where $\delta_{is}$ is 0 for type II and 1 for type I crystals, for which the subscripts in equation (35) should be omitted.

## 4 Double-slit interference in spontaneous parametric down-conversion

In this section, we consider double-slit interference in the SPDC case in which the input field is in the vacuum state. In Figure 1, the two down-converted beams generated from a crystal illuminate a double-slit and then are detected in the focal plane of the lens. We designate $a_m(x,t)$, $e_m(x,t)$, $e_m'(x,t)$, and $r_m(x,t)$ as the slowly varying field operators for the input surface $P_{in}$, the output surface $P_{out}$ of the crystal, the output plane of the double-slit $P_1$, and the detection plane $P_2$, respectively. Using equations (4) and (35), we may calculate the first- and second-order correlation functions for the field in the detection plane $P_2$.

The first-order correlation functions for the two beams are obtained to be

$$G_m^{(1)}(x_1,x_2) = M_m(x_1,x_2) \equiv \langle 0|r_m^\dagger(x_1,t)r_m(x_2,t)|0\rangle \quad (m=s,i) = \frac{k/f}{(2\pi)^2}\int dqd\Omega\,|V_m(q,\Omega)|^2 \times\widetilde{T}^*\left(\frac{kx_1}{f}-q\right)\widetilde{T}\left(\frac{kx_2}{f}-q\right). \quad (36)$$

$G_m^{(1)}(x,x)$ describes the one-photon interference pattern for beam $m$ in the detection plane.

Then we consider the second-order correlation function defined by equation (15), which now describes the spatial intensity correlation between the signal beam at position $x_2$ and the idler beam at position $x_1$. In the case of $x_1=x_2=x$, it describes a two-photon intensity distribution. For a type II crystal, intensity correlation of two orthogonally polarized beams can be measured experimentally by using a polarizing beam splitter (PBS) as shown in Figure 1b. For a type I crystal, however, the subscripts $s$ and $i$ should be omitted in equation (15). If a two-photon detector is available, one may observe the two-photon intensity distribution at position $x_1=x_2=x$. Otherwise, the realistic detection scheme for a type I crystal is shown in Figure 1a in which the intensity correlation is measured by two one-photon detectors at different positions $x_1$ and $x_2$.

For the vacuum state set in equation (15), by using equations (4) and (35b), we obtain the second-order

correlation

$$G^{(2)}(x_1,x_2)=M_i(x_1,x_1)M_s(x_2,x_2)+|N_{is}(x_1,x_2)|^2 + \delta_{is}\,|M(x_1,x_2)|^2. \quad (37)$$

$M_m(x_1,x_2)$ is given by equation (36), and

$$N_{mn}(x_1,x_2)=\frac{k/f}{(2\pi)^2}\int V_m(q,\Omega)U_n(-q,-\Omega) \times \widetilde{T}\left(\frac{kx_1}{f}-q\right)\widetilde{T}\left(\frac{kx_2}{f}+q\right)dqd\Omega \qquad (m\neq n=s,i). \quad (38)$$

For a type II crystal, equation (37) consists of two terms. The first term, which is separable in terms of both polarization and position, describes the contribution of two individual single-photon processes, whereas the second term describes two-photon interference effect related to photon entanglement. However, for a type I crystal, the third term introduces position correlation similar to the second term. As a matter of fact, the combination of the first and third terms in equation (37) identifies classical thermal correlation [21] (see also [23]).

In reference [24], intensity distribution and intensity correlation are defined by taking into account the detection system which has a finite detection area $S_d$ and a finite response time $T_d$. For perfect detection that the detection area $S_d$ is small enough for pattern resolution and the response time $T_d$ is much shorter than $1/\Omega_0$, the intensity distribution and the intensity correlation to be measured are proportional to the first- and the second-order correlation functions, respectively. For simplicity, we restrict our discussion to perfect detection.

We now consider the spatial symmetry of the first- and second-order correlation functions. Because of $|V_s(q,\Omega)|^2=|V_i(-q,-\Omega)|^2$ and $\widetilde{T}(q)=\widetilde{T}(-q)$, we obtain

$$M_s(x_1,x_2)=M_i(-x_1,-x_2) \quad (39)$$

for a type II crystal, and

$$M(x_1,x_2)=M(-x_1,-x_2)=M(x_2,x_1) \quad (40)$$

for a type I crystal, where the last equality in equation (40) is due to the real function $\widetilde{T}^*(q)=\widetilde{T}(q)$. Using equation (34b) and $\widetilde{T}(q)=\widetilde{T}(-q)$ in equation (38), we obtain

$$N_{mn}(x_1,x_2)=N_{nm}(x_2,x_1)=N_{nm}(-x_1,-x_2). \quad (41)$$

From equation (37), we arrive

$$\begin{aligned}G^{(2)}(-x_2,-x_1)&=M_i(-x_2,-x_2)M_s(-x_1,-x_1)\\&\quad+|N_{is}(-x_2,-x_1)|^2+\delta_{is}\,|M(-x_2,-x_1)|^2\\&=M_s(x_2,x_2)M_i(x_1,x_1)+|N_{si}(x_2,x_1)|^2\\&\quad+\delta_{is}\,|M(x_2,x_1)|^2\\&=G^{(2)}(x_1,x_2),\end{aligned} \quad (42)$$

where equations (39–41) are applied. In particular, this gives $G^{(2)}(x,x)=G^{(2)}(-x,-x)$. Therefore, for both type I and type II crystals, the two-photon interference pattern is symmetrical with respect to the symmetrical center of the double-slit.

In order to obtain analytical result for integrals (36) and (38), we discuss two bandwidth limits of the SPDC process: the broad and narrow bandwidths. In the broadband limit, ($q_0$ and $q_0'$) $\gg 2\pi/b$, $U_m(q,\Omega)$ and $V_m(q,\Omega)$ are much flatter in comparison with $\widetilde{T}(q)$ and we can set $U_m(q,\Omega)\approx U_m(0,\Omega)$ and $V_m(q,\Omega)\approx V_m(0,\Omega)$ in the integrals. By taking into account equations (20) and (21), equations (36) and (38) can be rewritten as

$$\begin{aligned}M_m(x_1,x_2)&=\frac{\eta_m}{\sqrt{2\pi}}\int dq\widetilde{T}^*\left(\frac{kx_1}{f}-q\right)\widetilde{T}\left(\frac{kx_2}{f}-q\right)\\&=\eta_m\widetilde{T}\left[\frac{k}{f}(x_2-x_1)\right]\qquad(m=s,i),\end{aligned} \quad (43)$$

and

$$N_{mn}(x_1,x_2)=\xi_{mn}\widetilde{T}\left[\frac{k}{f}(x_1+x_2)\right] \qquad (m\neq n=s,i), \quad (44)$$

respectively, where we define

$$\eta_m=(k/f)/(2\pi)^{3/2}\int|V_m(0,\Omega)|^2\,d\Omega$$

and

$$\xi_{mn}=(k/f)/(2\pi)^{3/2}\int V_m(0,\Omega)U_n(0,-\Omega)d\Omega.$$

In the broadband limit where the maximum entanglement in transverse wavevector occurs for two converted beams, we see again the position-correlation in the correlation functions. The first-order correlation equation (43) shows the same position-correlation as equation (19a) for the two-photon state with the maximum wavevector-entanglement. This makes one-photon intensity distribution in the detection plane $P_2$ homogeneous, $M_m(x,x)=\eta_m\widetilde{T}(0)$, i.e. the one-photon double-slit interference disappears completely.

In this limit, however, the second-order correlation (37) is obtained to be

$$G^{(2)}(x_1,x_2)=\eta_i\eta_s\left\{\widetilde{T}^2(0)+\delta_{is}\widetilde{T}^2\left[\frac{k}{f}(x_2-x_1)\right]\right\} + |\xi_{is}|^2\,\widetilde{T}^2\left[\frac{k}{f}(x_1+x_2)\right]. \quad (45)$$

The first term in {} comes from two individual single-photon double-slit processes which are now homogeneous. The second term in {} and the last term manifest explicitly position-correlation. To show two kinds of observation, $x_1=x_2=x$ and $x_1=-x_2=x$, the above equation is written as

$$G^{(2)}(x,x)=\eta_i\eta_s(1+\delta_{is})\widetilde{T}^2(0)+|\xi_{is}|^2\,\widetilde{T}^2\left(\frac{k}{f}2x\right), \quad (46)$$

and

$$G^{(2)}(x,-x) = (\eta_i\eta_s + |\xi_{is}|^2)\widetilde{T}^2(0) + \delta_{is}\eta_i\eta_s\widetilde{T}^2\left(\frac{k}{f}2x\right), \tag{47}$$

respectively. The former stands for the two-photon intensity distribution and the latter, the joint-intensity correlation at symmetric positions. Both equations (46) and (47) include a term $\widetilde{T}^2[(k/f)2x]$ which characterizes a sub-wavelength interference pattern by the factor of $\lambda/2$ in comparison with the ordinary interference shown by equation (9). Obviously, due to equation (46), the sub-wavelength interference for the two-photon intensity distribution can occur in both type I and type II crystals. However, equation (47) shows a sub-wavelength interference through joint-intensity measurement only for a type I crystal. As we indicated above, thermal correlation included in type I SPDC is responsible for this effect [21].

According to equations (46) and (47), the visibilities of fringes designated by $G^{(2)}(x,x)$ and $G^{(2)}(x,-x)$ are calculated to be

$$\mathcal{V}_1 = \frac{1}{1+2(1+\delta_{is})\theta}, \tag{48}$$

and

$$\mathcal{V}_2 = \frac{1}{3+2/\theta}, \tag{49}$$

respectively, where $\mathcal{V}_i = (G^{(2)}_{\max} - G^{(2)}_{\min})/(G^{(2)}_{\max} + G^{(2)}_{\min})$ $(i = 1, 2)$ and $\theta \equiv \eta_i\eta_s/|\xi_{is}|^2$. As the parameter $\theta$ is increased from a small quantity, $\mathcal{V}_1$ decreases monotonously from unity and $\mathcal{V}_2$ increases from zero up to 1/3. Since the parameter $\theta$ is related to the coupling strength $g$ of SPDC, we plot the visibilities as functions of $g$ in Figure 3, in which $\mathcal{V}_1$s for type II and type I crystals are indicated by the solid and dashed lines, respectively, and $\mathcal{V}_2$ for type I crystals is indicated by the dotted line. In Figure 3, the visibilities $\mathcal{V}_1$ of sub-wavelength interference fringe for both type I and II crystals reach perfectness in a weak coupling of SPDC, which generates approximately a two-photon entangled state. This effect has been observed experimentally [5,9,13,20]. The important fact is that, the sub-wavelength interference with a substantial visibility can exist even in very high gain SPDC, in which the beams contain a large amount of photons. This result is consistent with second-order temporal correlation in the plane-wave limit [19], and with ghost imaging and interference in the macroscopic realm [15].

$\mathcal{V}_2$ describes the visibility of sub-wavelength interference observed by a joint-intensity measurement. It exists only for type I crystals where $\theta \equiv \eta^2/|\xi|^2$. This visibility is trivial in low gain and increases with the gain of SPDC interaction. Therefore the nature of this kind of sub-wavelength interference is macroscopic without microscopic counterpart, reflecting the classical thermal correlation. In type I crystals, the two kinds of sub-wavelength interference compete for visibility, but can coexist in very high gain and reach the visibility about 20%.

For an ideal thermal light source, the visibility of sub-wavelength interference pattern is 1/3 which is irrelevant to the source intensity [23]. In the SPDC model, however, visibility $\mathcal{V}_2$ depends on the SPDC gain and, in particular, it tends to zero in the low gain limit. This is because that the second-order correlation function of SPDC consists of both the thermal correlation and the quantum entanglement. In the intensity correlation measurement with two detectors placed at symmetric positions $x_1 = -x_2 = x$, the quantum entanglement part shown by the second term in equation (45) contributes an additional background to the interference pattern. In the low gain limit, the quantum entanglement dominates the second-order correlation function of SPDC, and in fact the down-converted fields are approximately in a two-photon entangled state. Therefore, the sub-wavelength interference related to the thermal correlation disappears.

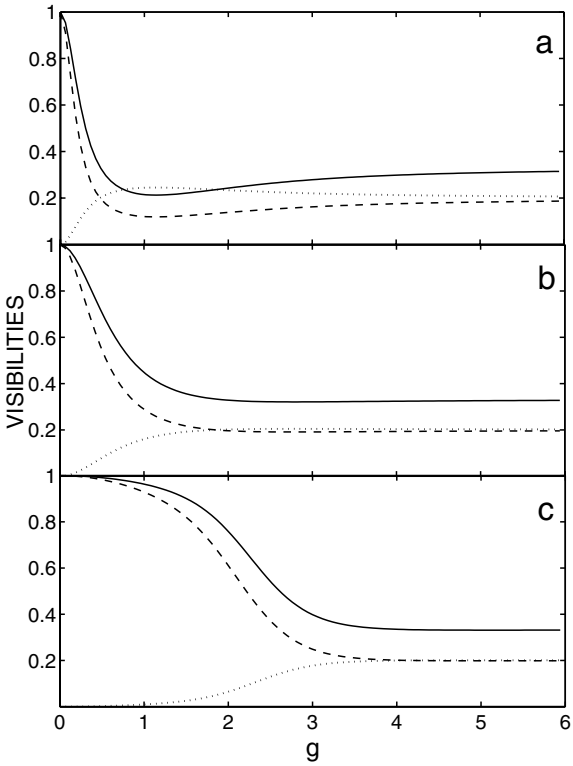


**Fig. 3.** Visibilities $\mathcal{V}_1$ and $\mathcal{V}_2$ versus the gain of SPDC for different collinear phase-mismatching (a) $\Delta_0 = -5.85$; (b) $\Delta_0 = 0$; and (c) $\Delta_0 = 5.85$. Solid and dashed lines designate $\mathcal{V}_1$ for type II and type I crystals, respectively; dotted line designates $\mathcal{V}_2$ for a type I crystal.

In the opposite limit, we assume that the SPDC has a very narrow bandwidth $q_0 \ll 2\pi/b$. Extremely when $q_0 \to 0$, the transfer coefficient $V_m(q,\Omega)$ $(m = s, i)$ tends to the delta function

$$V_m(q,\Omega) \to V_m(0,\Omega)\delta(q). \tag{50}$$

Equations (36) and (38) are respectively written as

$$M_m(x_1,x_2) = \frac{1}{\sqrt{2\pi}}\eta_m\widetilde{T}\left(\frac{kx_1}{f}\right)\widetilde{T}^\star\left(\frac{kx_2}{f}\right), \tag{51}$$

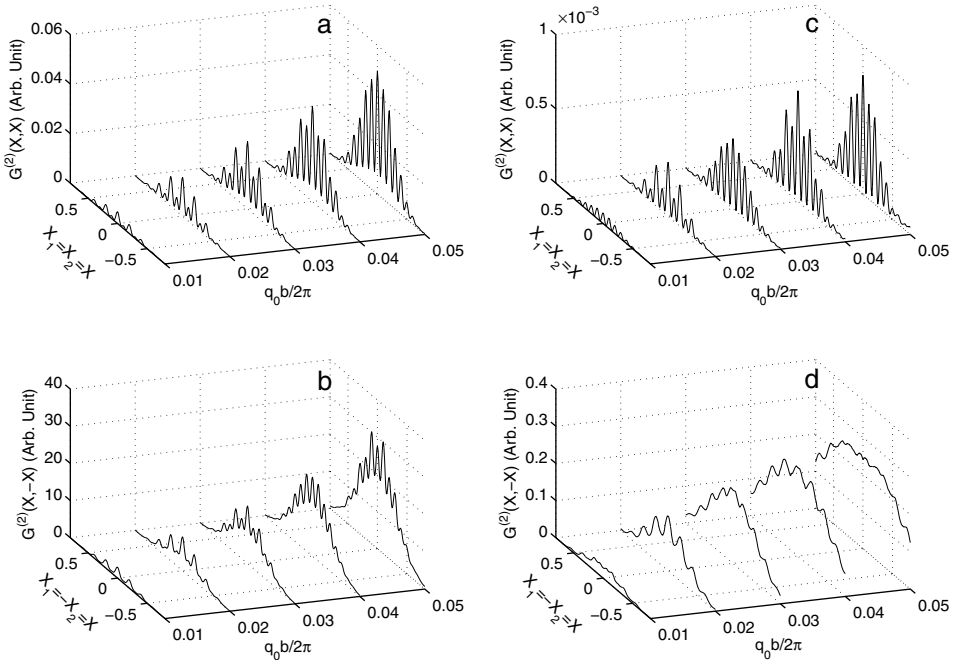


**Fig. 4.** Two-photon interference patterns versus the normalized bandwidth of SPDC $q_0 b/(2\pi)$: (a) $G^{(2)}(X,X)$ for a type I crystal; (b) $G^{(2)}(X,-X)$ for a type I crystal; (c) $G^{(2)}(X,X)$ for a type II crystal; and (d) $G^{(2)}(X,-X)$ for a type II crystal, where $X = xkb/(2\pi f)$ is the normalized transverse position in the detection plane. The gains are set as $g = (1/2)\log 1.5$ in (a) and (c), and $g = (1/2)\log 10$ in (b) and (d). The walk-off bandwidths $\Omega_0' = \Omega_0/10$, $q_0' = q_0/10$ are set in (c) and (d) for a type II crystal. In Figures 4–8, the phase matching $\Delta_0 = 0$ and the double-slit parameter $b/d = 0.2$ are taken.

and

$$N_{mn}(x_1,x_2) = \frac{1}{\sqrt{2\pi}}\xi_{mn}\widetilde{T}\left(\frac{kx_1}{f}\right)\widetilde{T}\left(\frac{kx_2}{f}\right). \quad (52)$$

In this limit, the position-correlation disappears completely. The second-order correlation is then

$$G^{(2)}(x_1,x_2) = \frac{1}{2\pi}\left[(1+\delta_{is})\eta_i\eta_s + |\xi_{is}|^2\right] \times \widetilde{T}^2\left(\frac{kx_1}{f}\right)\widetilde{T}^2\left(\frac{kx_2}{f}\right). \quad (53)$$

Therefore, the one-photon intensity distribution $M_m(x,x)$ and the second-order correlation function $G^{(2)}(x_1,x_2)$ in the plane $P_2$ are the same as the case for the coherent state. This can be understood by the fact that the two down-converted beams have no more correlation in transverse wavevector.

We plot the two-photon interference patterns by varying the bandwidth $q_0$ of SPDC process in Figure 4, in which Figures 4a and 4b (4c and 4d) are for a type I (type II) crystal. In Figures 4a and 4c, a low gain SPDC, $g = (1/2)\log 1.5$ (with the amplification rate 1.5) is taken in two-photon intensity measurement so that the sub-wavelength interference with a better visibility is achieved when the normalized bandwidth $q_0 b/(2\pi)$ is increased. The fringe patterns for two types of crystals are very alike but the fringe intensity for a type II crystal is much lower. The feature of type II phase matching does not affect spatial correlation but simply lowers the number of generated photon pairs [26]. Figures 4b and 4d show the interference patterns for joint-intensity measurement of two one-photon detectors placed at symmetric positions. The sub-wavelength interference can be observed only for a type I crystal when the gain of SPDC is higher, for instance, $g = (1/2)\log 10$ (with the amplification rate 10) is taken in the figures. Though the visibilities are lower, the intensities of the patterns are getting much higher. This is also true for the case of two-photon intensity measurement. The three plots of Figures 4a–4c show that the bandwidth of SPDC governs sub-wavelength interference. When the bandwidth of SPDC is very small, the two converted beams are de-correlated in transverse wavevector and hence the sub-wavelength interference disappears.

## 5 Double-slit interference in stimulated parametric down-conversion

In the stimulated optical parametric process, a signal beam is injected into a nonlinear crystal and then amplified. The nonlinear crystal becomes an optical parametric amplifier (OPA). We assume a stationary plane-wave beam in a coherent state as input

$$\langle \widetilde{a}_s(q,\Omega)\rangle = 2\pi A\delta(q-Q)\delta(\Omega), \quad (54)$$

where $Q$ designates the transverse wavevector of the input beam deviated from the normal incidence. For a type II crystal, we name the input beam as the signal which can be identified by polarization, while the idler beam is in the vacuum state. For a type I crystal, the subscript $s$ in (54) is omitted. Considering the input beam described by equation (54), we calculate the first-order correlation in the plane $P_2$

$$G_m^{(1)}(x_1,x_2) = W_m^*(x_1,Q)W_m(x_2,Q) + M_m(x_1,x_2) \quad (m=s,i), \quad (55)$$

where

$$W_s(x,Q) = A\sqrt{k/f}U_s(Q,0)\widetilde{T}(kx/f-Q) \quad (56a)$$

$$W_i(x,Q) = A\sqrt{k/f}V_i(-Q,0)\widetilde{T}(kx/f+Q) \quad (56b)$$

for a type II crystal, and

$$W(x,Q) = A\sqrt{k/f}[U(Q,0)\widetilde{T}(kx/f-Q) + V(-Q,0)\widetilde{T}(kx/f+Q)] \quad (57)$$

for a type I crystal. $M_m(x_1,x_2)$ has been defined by equation (36). In equation (55), the first and second terms show contributions coming from the stimulated and the spontaneous processes, respectively. Obviously, the stimulated part shows the first-order coherence because of the separability of spatial variables. Nevertheless, when the input beam is strong enough, the spontaneous process can be neglected. $G_m^{(1)}(x,x) \simeq |W_m(x,Q)|^2$ describes an amplified double-slit interference pattern in comparison with the case when the crystal is taken away.

For a type I crystal, however, the one-photon interference pattern contributed by the stimulated process is written as

$$|W(x,Q)|^2 = \frac{kA^2}{f}\left\{|U(Q,0)|^2\widetilde{T}^2\left(\frac{kx}{f}-Q\right) + |V(-Q,0)|^2\widetilde{T}^2\left(\frac{kx}{f}+Q\right) + \left[U(Q,0)V^*(-Q,0)\widetilde{T}\left(\frac{kx}{f}-Q\right)\widetilde{T}\left(\frac{kx}{f}+Q\right)+\text{c.c.}\right]\right\}. \quad (58)$$

The first and second terms correspond to the two interference patterns generated by the two stimulated beams, i.e. the signal beam with the transverse wavevector $Q$ and the idler beam with $-Q$. The third term represents an additional coherent superposition of the two stimulated fields. As a result, the interference pattern can be different from the ordinary one due to this additional "interference term". We plot the stimulated one-photon interference patterns for a type I crystal in Figure 5. For the normal incidence case $Q = 0$, the interference pattern shown in Figure 5a is the same as the ordinary one indicated by equation (9) with the exception of a spontaneous background. When the transverse wavevector $Q$ of the input beam is increased, the interference fringe fades at $Qb/(2\pi) = 0.12$ in Figure 5b, and is then revived at $Qb/(2\pi) = 0.4$ in Figure 5c. As the input beam is well tilted in incidence, $Qb/(2\pi) = 0.9$ in Figure 5d for instance, the signal and idler patterns are separated in space.

For a type II crystal, the input signal beam creates two interference patterns: one for the outgoing signal beam with the amplification ratio $|U_s(Q,0)|^2$ and the other for the outgoing idler beam with the amplification ratio $|V_i(-Q,0)|^2$ [27]. According to equations (56), these two patterns are the same as the ordinary one (see Eq. (9)) and can be identified by polarization. Figure 6 shows the stimulated one-photon interference patterns for a type II crystal. We can see that when the transverse wavevector $Q$ of the input beam is increased, the signal and idler interference patterns are separated in space. However, the background of the patterns formed by the spontaneous radiation is spatially unbalanced because of the odd walk-off term $q/q_0'$ in type II phase matching.

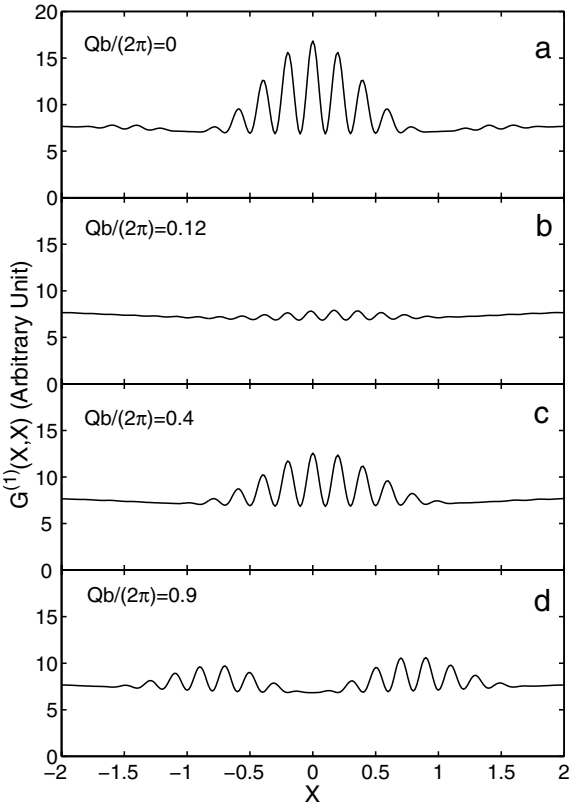


**Fig. 5.** Stimulated one-photon interference patterns for a type I crystal. The normalized transverse wavevector of the input field are set as $Qb/2\pi = 0$, 0.12, 0.4 and 0.9 for (a), (b), (c) and (d), respectively. The parameters are taken as $q_0 b/2\pi = 2$, $kb\Omega_0/4\pi^2 f = 1$, $(2kb^2/\pi f)A^2 = 1$ and $g = (1/2)\log 10$.

We go through a long derivation, using the unitary transformation (24) and the bosonic commutation relation, and obtain the second-order correlation function in the detective plane $P_2$

$$G^{(2)}(x_1,x_2) = [|W_i(x_1,Q)|^2 + M_i(x_1,x_1)][|W_s(x_2,Q)|^2 + M_s(x_2,x_2)] + [W_i(x_1,Q)W_s(x_2,Q)N_{is}^*(x_1,x_2) + \text{c.c.}] + |N_{is}(x_1,x_2)|^2 + \delta_{is}[W^*(x_1,Q)W(x_2,Q)M(x_1,x_2) + \text{c.c.}] + \delta_{is}|M(x_1,x_2)|^2. \quad (59)$$

Again, equation (59) can describe two types of crystals. For a type I crystal, the subscripts $i$ and $s$ are omitted and $\delta_{is} = 1$, whereas for a type II crystal $\delta_{is} = 0$. Similar to equation (37), the first term is the product of the two one-photon interference patterns for the outgoing beams. The third and fifth terms refer to the spontaneous process. However, the second and the fourth terms exhibit the interference terms between the stimulated and spontaneous processes. The result is similar to the discussion of image amplification in OPA where $W(x)$ describes an amplified image [28]. The terms related to the stimulated process do not contain the position-correlation, and will not bring about sub-wavelength interference.

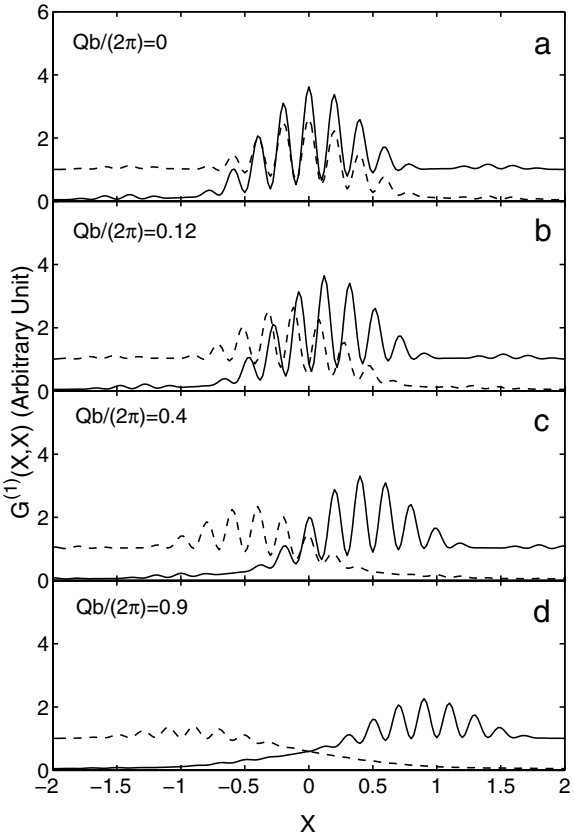


**Fig. 6.** Stimulated one-photon interference patterns of the signal (solid line) and idler beams (dashed line) for a type II crystal. The normalized transverse wavevector of the input field are set as $Qb/(2\pi) = 0$, 0.12, 0.4 and 0.9 for (a), (b), (c) and (d) respectively. We take $q_0' = q_0/10$, $\Omega_0' = \Omega_0/10$, and the other parameters the same as in Figure 5.

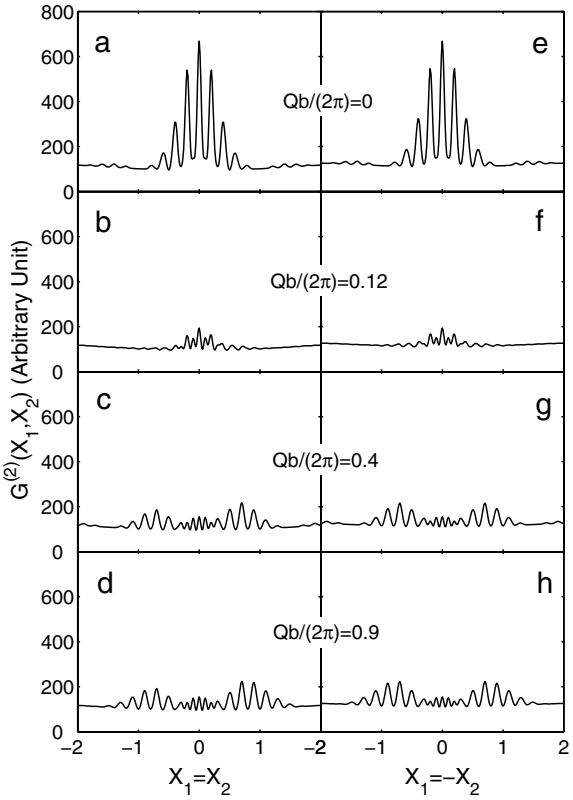


**Fig. 7.** Stimulated two-photon interference patterns for a type I crystal where (a–d) are for the two-photon intensity distribution $X_1 = X_2$ and (e–h) for the joint-intensity measurement at symmetric positions $X_1 = -X_2$. We set the normalized transverse wavevector of the input field $Qb/(2\pi) = 0$, 0.12, 0.4 and 0.9 for (a, e), (b, f), (c, g) and (d, h), respectively. The parameters are the same as in Figure 5.

In Figure 7, we plot the stimulated two-photon interference patterns for a type I crystal by setting several values of input direction. Figures 7a–7d and 7e–7h show the two-photon intensity measurement and the joint-intensity measurement, respectively. For the normal incidence case $Q = 0$, two kinds of observation exhibit the same pattern. Similar to the one-photon interference in a type I crystal, for the two kinds of observation, the interference patterns contributed by the stimulated fields alternately fade out and in when the transverse wavevector $Q$ of the input beam is increased. For a large $Q$, the two stimulated patterns are well apart while the sub-wavelength interference patterns contributed by the spontaneous process appear in the center.

For a type II crystal, the two-photon measurement can be performed by the scheme shown in Figure 1b. Figures 8a–8d and 8e–8h show the joint-intensity measurement for $x_1 = x_2$ and $x_1 = -x_2$, respectively. When the transverse wavevector $Q$ is increased, the interference pattern for $x_1 = x_2$ expands until it is divided into two stimulated patterns and leaves the spontaneous one in the center. As for the joint-intensity measurement $x_1 = -x_2$, however, the pattern moves away from the center with increasing the input transverse wavevector. These features differ from that of type I crystals due to the polarization distinguishability between the signal and idler photons. For the first observation, the fade pattern does not exist since there is no additional "interference term" between the two stimulated beams. However, in the second observation, only one pattern appears even for a large $Q$ simply because of the polarization-sensitive joint-intensity measurement which is performed through the PBS.

## 6 Conclusions

In summary, we formulate the first- and second-order correlation functions in the Young's double-slit interference for both spontaneous and stimulated parametric down-conversions. We show that the sub-wavelength two-photon interference can occur macroscopically in a general spontaneous parametric process. Even if for a very high gain of SPDC, in which the converted beams contain a huge number of photons, the sub-wavelength interference pattern is intensive with a solid visibility. This makes the sub-wavelength lithography technology practicable. Moreover, for a type I crystal, the sub-wavelength interference can exist by performing a joint-intensity measurement with

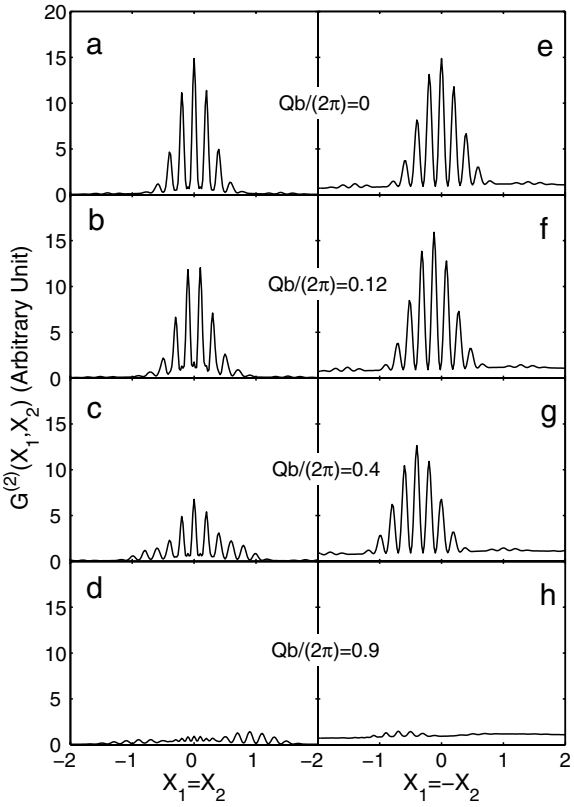


**Fig. 8.** Stimulated two-photon interference patterns for a type II crystal where (a–d) are for the two-photon intensity distribution $X_1 = X_2$ and (e–h) for the joint-intensity measurement at symmetric positions $X_1 = -X_2$. The parameters are the same as in Figure 6.

two one-photon detectors placed at symmetric positions. Since this effect occurs only in a higher gain of SPDC, it reflects the macroscopic nature. Our theoretical analysis shows that the sub-wavelength interference originates from classical thermal correlation, playing a similar role as quantum entanglement as already shown in [21] (see also [23]). In the early time of quantum optics, the second-order temporal and spatial correlation of thermal light was shown in the famous Hanbury-Brown and Twiss experiment [29]. From photonic viewpoint, two thermal photons travel together more likely than they are apart. An intuitive understanding could be: bunched photons in thermal light play likely a similar role as biphoton. However, the more convinced explanation should refer to the similarity of the second-order correlation between the entangled photons and the thermal light [21] (see also [23]).

In the stimulated process, one-photon and two-photon interference patterns generated by the outgoing stimulated beams can be amplified. For a type I crystal, the two stimulated beams are indistinguishable in the collinear case and result in a secondary interference which may fade the fringe.

This research was supported by the National Program of Fundamental Research No. 2001CB309310 and the National Natural Science Foundation of China, Project No. 10074008 and No. 60278021.

## References

1. D.V. Strekalov, A.V. Sergienko, D.N. Klyshko, Y.H. Shih, Phys. Rev. Lett. **74**, 3600 (1995)
2. P.H.S. Ribeiro, S. Pádua, J.C. Machado da Silva, G.A. Barbosa, Phys. Rev. A **49**, 4176 (1994)
3. P.H. Souto Ribeiro, G.A. Barbosa, Phys. Rev. A **54**, 3489 (1996)
4. G.A. Barbosa, Phys. Rev. A **54**, 4473 (1996)
5. E.J.S. Fonseca, C.H. Monken, S. Pádua, Phys. Rev. Lett. **82**, 2868 (1999)
6. E.J.S. Fonseca, C.H. Monken, S. Pádua, G.A. Barbosa, Phys. Rev. A **59**, 1608 (1999)
7. E.J.S. Fonseca, P.H. Souto Ribeiro, S. Pádua, C.H. Monken, Phys. Rev. A **60**, 1530 (1999); E.J.S. Fonseca, Z. Paulini, P. Nussenzveig, C.H. Monken, S. Pádua, Phys. Rev. A **63**, 043819 (2001)
8. B.E.A. Saleh, A.F. Abouraddy, A.V. Sergienko, M.C. Teich, Phys. Rev. A **62**, 043816 (2000)
9. M. D'Angelo, M.V. Chekhova, Y. Shih, Phys. Rev. Lett. **87**, 013602 (2001)
10. A.F. Abouraddy, M.B. Nasr, B.E.A. Saleh, A.V. Sergienko, M.C. Teich, Phys. Rev. A **63**, 063803 (2001)
11. A.F. Abouraddy, B.E.A. Saleh, A.V. Sergienko, M.C. Teich, J. Opt. B: Quant. Semiclass. Opt. **3**, S50 (2001)
12. S.P. Walborn, M.O. Terra Cunha, S. Pádua, C.H. Monken, Phys. Rev. A **65**, 033818 (2002)
13. R. Shimizu, K. Edamatsu, T. Itoh, Phys. Rev. A **67**, 041805 (2003)
14. G. Brida, E. Cagliero, G. Falzetta, M. Genovese, M. Gramegna, E. Predazzi, Phys. Rev. A **68**, 033803 (2003)
15. A. Gatti, E. Brambilla, L.A. Lugiato, Phys. Rev. Lett. **90**, 133603 (2003)
16. J. Jacobson, G. Björk, I. Chuang, Y. Yamamoto, Phys. Rev. Lett. **74**, 4835 (1995)
17. A.N. Boto, P. Kok, D.S. Abrams, S.L. Braunstein, C.P. Williams, J.P. Dowling, Phys. Rev. Lett. **85**, 2733 (2000)
18. G.S. Agarwal, R.W. Boyd, E.M. Nagasako, S.J. Bentley, Phys. Rev. Lett. **86**, 1389 (2001)
19. E.M. Nagasako, S.J. Bentley, R.W. Boyd, G.S. Agarwal, Phys. Rev. A **64**, 043802 (2001)
20. K. Edamatsu, R. Shimizu, T. Itoh, Phys. Rev. Lett. **89**, 213601 (2002)
21. A. Gatti, E. Brambilla, M. Bache, L.A. Lugiato, Phys. Rev. A **70**, 013802 (2004), `arXiv:quant-ph/0405056`
22. A. Gatti, E. Brambilla, M. Bache, L.A. Lugiato, Phys. Rev. Lett. **93**, 093602 (2004), `arXiv:quant-ph/0307187`
23. K. Wang, De-Zh. Cao, Phys. Rev. A **70**, 041801(R) (2004)
24. M.I. Kolobov, L.A. Lugiato, Phys. Rev. A **52**, 4930 (1995)
25. I.V. Sokolov, M.I. Kolobov, L.A. Lugiato, Phys. Rev. A **60**, 2420 (1999)
26. E. Brambilla, A. Gatti, M. Bache, L.A. Lugiato, Phys. Rev. A **69**, 023802 (2004)
27. A. Gatti, E. Brambilla, L.A. Lugiato, M.I. Kolobov, Phys. Rev. Lett. **83**, 1763 (1999)
28. K. Wang, G. Yang, A. Gatti, L.A. Lugiato, J. Opt. B: Quant. Semiclass. Opt. **5**, S1 (2003)
29. R. Hanbury-Brown, R.Q. Twiss, Nature **177**, 27 (1956)